DOI: 10.1002/chem.200903347

Fabrication of Large-Scale Hierarchical ZnO Hollow Spheroids for Hydrophobicity and Photocatalysis

Arun Kumar Sinha, Mrinmoyee Basu, Mukul Pradhan, Sougata Sarkar, and Tarasankar Pal*[a]

Abstract: We report here the preparation of a crystalline, pure hexagonal phase of ZnO as hollow 500–800 nm spheroids in the presence of organic bases, such as pyridine, using zinc acetate as the precursor salt. The spheroids exhibit unique 3D hierarchical architectures, like cocoons, and demonstrate improved superhydrophobic (water contact angle, 150°) character due to the inherited air-trapped capillarity within the cocoon structure. The simple synthetic strategy used in this process is modified hydrothermolysis (MHT), which represents a general approach and may contribute to the formation mechanism of the hollow nanostructures with highly improved porosity. Depending on the concentration of the precursor salt, it has been possible to cover glass plates or the inner wall of a reaction vessel with ZnO nanocrystals. A low salt concentration (<0.01 M) allows the easy preparation of a superhydrophobic glass surface, whereas a high salt concentration (>0.01 M) results in the precipitation of cocoons at the bottom of the reaction vessel as a solid mass together with a deposited thin film of ZnO nanocrystals covering the inner wall of the glass vessel. The thickness of the film successively grows through repetitive hydrothermolysis processes for which a low salt concentration (<0.01 M) was employed. Because of the hollow cocoon-like morphology, the surface area of the film is greatly increased, which makes it accessible for functionalization by incoming substrates from both sides (internally and externally) and helps to drive a competent photocatalytic dye degradation pathway. The heterocyclic base pyridine exclusively develops cocoons. Thus, the mechanism of self-aggregation of ZnO nanocrystals under MHT reaction conditions has been studied and the characterization of the compounds has been supported with physical measurements.

Keywords: hexagonal ZnO · nanococoon · photocatalysis · superhydrophobicity · template synthesis

Introduction

In nanoscience and nanotechnology, hollow structured materials have received great attention in the general synthesis of functional materials because of their important applications in vastly different fields.[1] Among the known preparative methods for these structured materials, templating has been shown to be an effective approach to tailor-make the interior hollow spaces. Both hard templates, such as inorganic or organic cores, and soft templates, such as vesicles and micelles in emulsions or ionic liquids, provide efficient support.[2] To explore new capabilities of templating methods, researchers have further investigated the self-assembly of nanounits on the interface or surface of the templates as part of the general "bottom-up" paradigm adopted in nanotechnology. Herein we have designed a bubble-template approach to generate crystalline, self-assembled hierarchical structures of ZnO thin film as cocoons.

The wetting behavior of a solid surface by a liquid is a very important aspect of surface chemistry, which may have a variety of practical applications.[3] When a liquid droplet softly touches a solid substrate, it will either remain as a droplet or spread out on the surface to form a thin liquid film: a property normally characterized by using contact angle (CA) measurements. For a solid substrate, when the CA of water or oil is larger than 150° it is called superhydrophobic. On the other hand, when the CA of water or oil on a surface is almost 0°, it is called superhydrophilic.[4] Inspired by superhydrophobic living organisms, such as lotus

[a] A. K. Sinha, M. Basu, M. Pradhan, S. Sarkar, Prof. T. Pal
Department of Chemistry, Indian Institute of Technology
Kharagpur, Kharagpur-721302 (India)
Fax: (+91) 03222-255303
E-mail: tpal@chem.iitkgp.ernet.in

Supporting information for this article is available on the WWW under http://dx.doi.org/10.1002/chem.200903347.

leaves and legs of water-striders, artificial surfaces with superhydrophobic properties are being fabricated by two different approaches: by creating micro/nanostructures on hydrophobic substrates or by chemically modifying a micro/nanostructured surface with materials of low surface free energy.[5] In this way, various methods for attaining surface roughness have been proposed, such as crystallization control, electrochemical deposition, and chemical vapor deposition.[6] Superhydrophilic surfaces have also been fabricated by increasing both the surface roughness and the surface free energy. The mechanism here is commonly referred to as a 2D or 3D capillary effect.

To mimic the hydrophobicity of naturally created templates, metal oxide thin films have come under study due to their stability. It has been discovered that metal oxide thin films can also show UV-light-switchable hydrophobic/-philic characteristics. In 1997, Fujishima et al. reported the TiO_2 anatase thin film on a glass substrate to have a water CA of 72° before UV irradiation; after irradiation the water droplets spread out as a film resulting in a CA of 0°.[7] A remarkable, controllable surface wettability that shows reversible hydrophobicity/-philicity under UV irradiation, which is a fascinating challenge in surface chemistry, is observed for our ZnO thin film. It has been shown that ZnO thin films can be switched back and forth between superhydrophilic and hydrophobic, controlled by the geometrical pattern of the nanostructure, resulting in changes to the surface chemistry. Only a few reports have focused on the hydrophobicity of shape-controlled ZnO nanocrystals, such as rods, wires, particles, and tubes, at a particular orientation. We now report, for the first time, the UV-light-controlled superhydrophobicity of a nanococoon ZnO surface.

The cooperation of the hollow nanostructures, the orientation of the crystal planes, the air pocket in the nanococoon, and the surface photosensitivity are considered to be responsible for the observed behavior. This unique nanococoon morphology, which inherits an air-trapped 3D capillarity seems to be responsible for the water-repelling property arising from the rough ZnO surface.

Herein, we show the sticking of a novel nanococoon architecture, with an encapsulated air compartment in the cavity of ZnO nanoparticle assembly, onto the surface of glass plate. The improved hydrophobicity of the ZnO thin film has been fabricated with a low-cost method. In addition, this film has a self-cleaning property; it has a high CA value (150°), which is reduced to 0–15° under UV irradiation, however, the original value is reversibly restored when the film is kept in the dark.

Results and Discussion

Characterization of the nanocrystals: Recent developments in nanoparticle synthesis place emphasis on controlling the size and shape of particles, taking into account reproducibility and structural complexity. We have tried to develop a methodology for the synthesis of nanococoon-shaped ZnO with a high surface area. The synthesized ZnO nanocrystals are characterized by using different physical methods, such as FTIR, UV-visible spectroscopy, XRD, Raman spectroscopy, field-emission SEM (FESEM), energy dispersive X-ray spectroscopy (EDS) and TEM.

The FTIR absorption spectrum of the ZnO nanococoon is shown in Figure 1b: a strong, broad peak for Zn–O was found at $\nu = 494\ cm^{-1}$, and the strong peaks of the COO^-

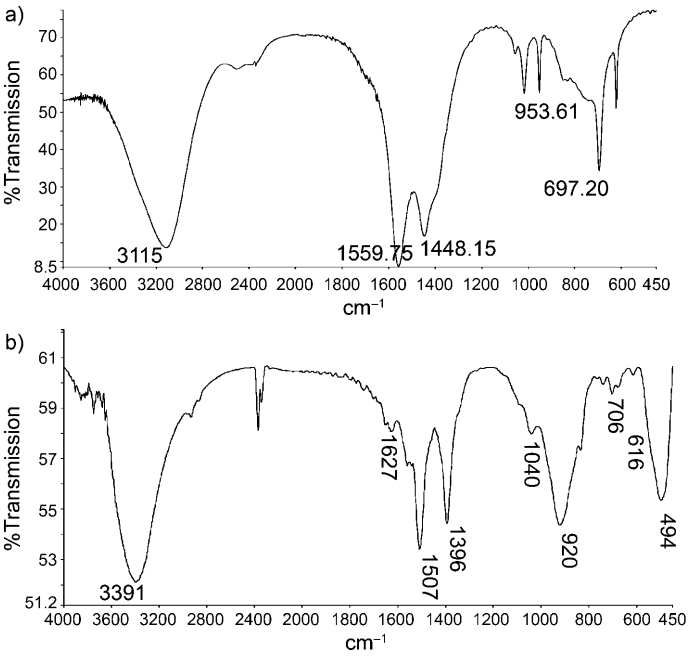

Figure 1. The FTIR spectrum of solid $Zn(CH_3COO)_2{\cdot}2H_2O$ (a) and ZnO nanococoon spheroids (b) in a KBr pellet.

groups were observed at $\nu = 1390$–$1600\ cm^{-1}$. This indicates that the surface of the obtained ZnO nanococoon is covered with acetate ligands. The band at $\nu = 3391\ cm^{-1}$ is due to the O–H moieties in the sample and those at $\nu = 2800$–$3000\ cm^{-1}$ to the C–H stretching frequencies. The bands appearing at $\nu = 1507$ and $1396\ cm^{-1}$ are due to C=O bonds from the bridging type metal–acetate bonding in the ZnO nanoarchitecture. The building units of the nanococoon are the ZnO nanocrystals, which are chelated to one another. Because of the chelated zinc compound, the nanococoon structure shows strong absorptions at $\nu = 920$ and $1040\ cm^{-1}$ due to the stretching vibrations of C–O bonds of the acetate ligands. When the ZnO sample was annealed at 450 °C, absorption bands corresponding to the organic acetate species and hydroxyl groups were no longer observed, indicating the complete removal of chelating species and hydroxyl groups. Thus ZnO is purified through annealing.[8]

The optical properties of a thin film of the ZnO nanocrystals were investigated by UV-visible absorption spectroscopy. The peak positioned at $\lambda = 350$ nm for ZnO is reported and shown in Figure 2. Raman scattering measurements were performed to investigate the properties of the ZnO

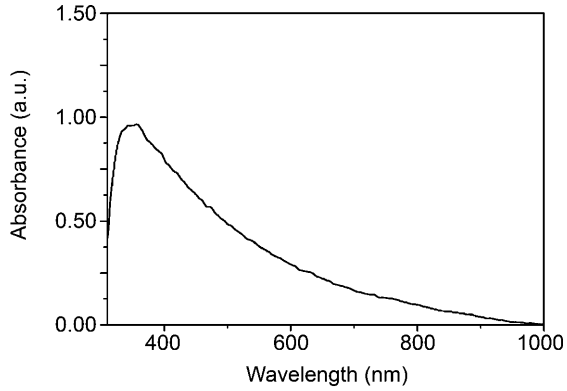

Figure 2. The UV-visible spectrum of ZnO nanococoon spheroids as a thin film.

nanococoons at room temperature (Figure 3a). The remarkable E_{2H} mode of ZnO is located at 440 cm^{-1}, which corresponds to the characteristic band of the hexagonal wurtzite

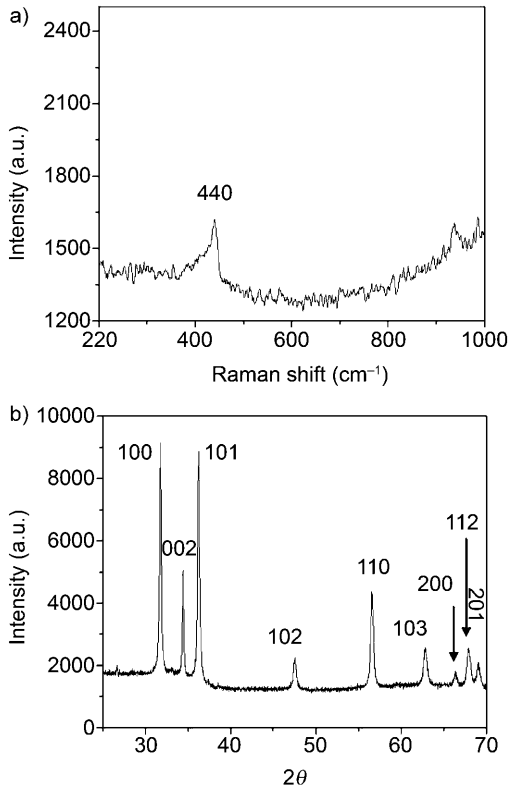

Figure 3. The Raman spectrum (a) and XRD pattern (b) of the typical ZnO hollow spheroids.

phase.[9] The experimental XRD spectrum of the ZnO nanococoon is shown in Figure 3b. All strong peaks can be indexed to the pure hexagonal wurtzite structure of ZnO, which agrees well with the reported data (JCPDS no. 79-0206) with no evidence of other ZnO phases.[10] The typical hollow spheroids were scanned for X-ray photoelectron spectroscopy (XPS), and their survey curves are shown in Figure 4a and b. The binding energies of both Zn $2p_{1/2}$ (1048.17 eV) and Zn $2p_{3/2}$ (1024.98 eV) are indicated in Figure 4b and are slightly larger than the values of Zn in the

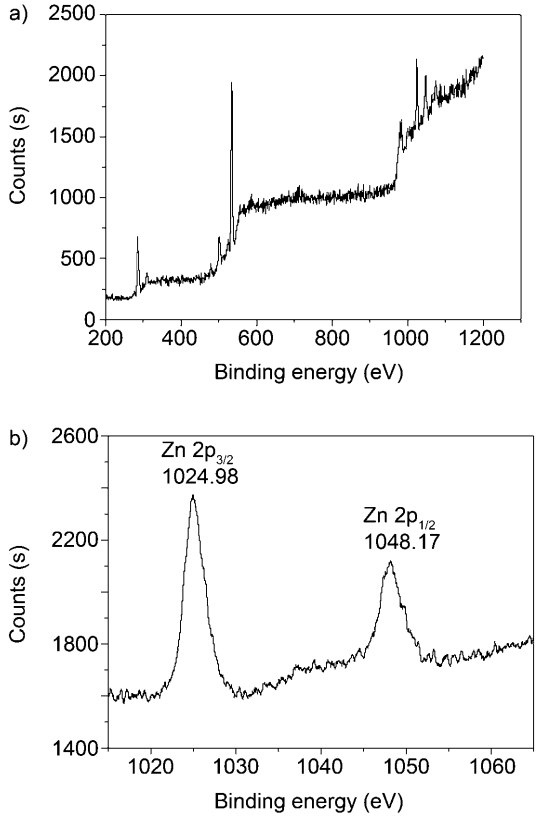

Figure 4. Survey scan for the ZnO nanococoon (a) and the XPS spectrum of Zn 2p core-level (b).

bulk ZnO, indicating that Zn is in the formal Zn^{II} valence state within an oxygen-deficient environment.[11] Figure 5 shows a FESEM image of the synthesized product at different magnifications. The product mainly contains uniform hollow spheroids with diameters of about 500–800 nm with a rough surface. The interior detail of the spheroids can be clearly examined through a broken surface, which can be obtained by ultrasonication or heating of the spheroids (Figure 6a–c). These interior spaces are similar to those of cocoons found in nature (Figure 6d).

The morphologies of the ZnO hollow cocoons obtained under typical conditions were examined by TEM analysis (Figure 7). As shown in Figure 7a, the ZnO morphology is spheroidal with diameters ranging from 500–800 nm and the interior of these spheroids are hollow, which indicates that the prepared product forms aesthetically beautiful sub-micrometer hollow cocoons. TEM observation shows that the shell thickness is about 15–20 nm, and the surface of the hollow spheroids are composed of innumerable ZnO nanoparticles, as shown in the highly magnified TEM and FESEM images (see Figure S1 in the Supporting Informa-

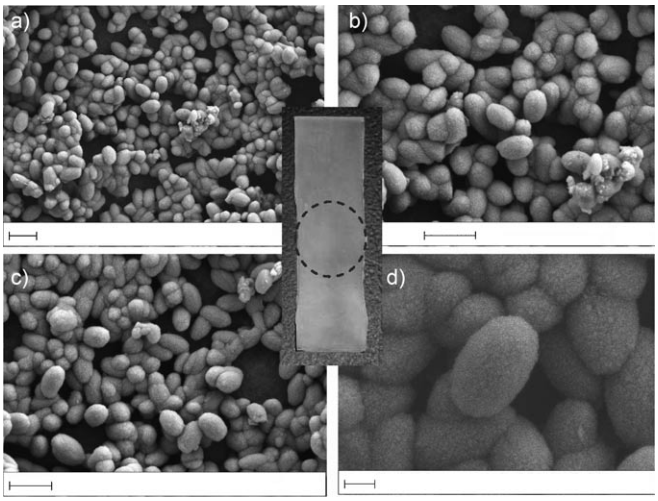

Figure 5. FESEM images of ZnO nanococoons as thin films on a glass surface at different magnifications. $Zn(CH_3COO)_2{\cdot}2H_2O$ (2.5 mL 0.01 M) was hydrothermolyzed in the presence of pyridine (0.1 M) in an MHT reactor. Digital photograph of ZnO thin film on a rectangular micro glass slide is shown in the middle. Scale bars: a) 1 μm, b) 1 μm, c) 1 μm, and d) 200 nm.

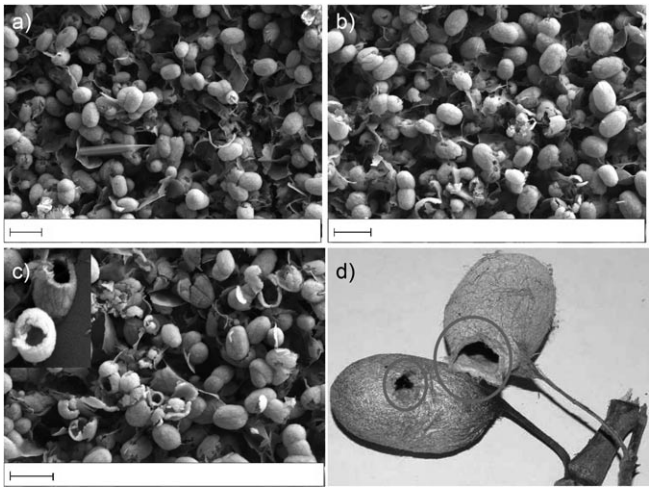

Figure 6. FESEM images of ZnO nanococoons as a powder at different magnifications. $Zn(CH_3COO)_2{\cdot}2H_2O$(2.5 mL 0.01 M) was hydrothermolyzed in the presence of pyridine (0.5 mL 0.1 M) in an MHT reactor; ZnO appeared as precipitate. FESEM images of the as-synthesized hollow cocoons after ultrasonic treatment for 15 min (a) and heat treatment in dry conditions (b). FESEM image of an unveiled spheroid clearly indicating the hollow structure of the spheroids (c), which is similar to that of cocoons found in nature (d). All scale bars are 1 μm.

tion). The hollow cocoons might serve as microchemical reactors owing to the void space, which has an inner diameter of 470–770 nm. The ratio of $Zn(CH_3COO)_2{\cdot}2H_2O$ to pyridine was varied to determine the optimal conditions. In the Supporting Information (Figure S2), the TEM images of the nanococoons prepared by using different $Zn(CH_3COO)_2{\cdot}2H_2O$/pyridine ratios are shown. The composition of the product was confirmed by EDS; in the EDS spectrum of a typical product, only peaks for O and Zn

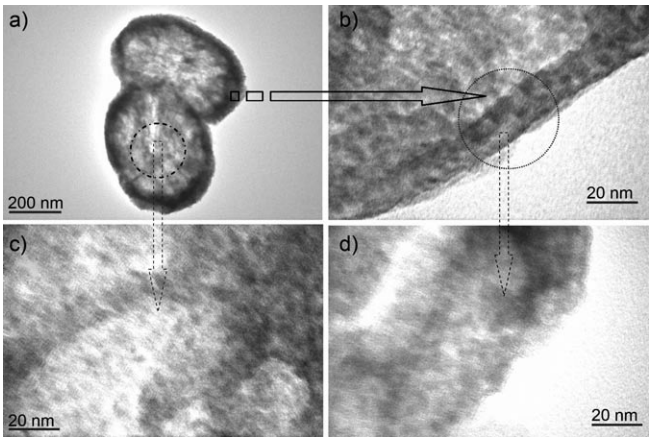

Figure 7. HRTEM images of a ZnO nanocrystal at different positions and different magnifications. The ZnO nanococoon structure (a), the determination of the thickness of the ZnO wall (b), the center of the ZnO nanostructure at high magnification (c), and the border of the ZnO nanocrystal at high magnification (d).

were observed (the Cu and Si peaks in the spectrum are due to background from the copper TEM grid), which confirms that the hollow spheroids are composed of pure ZnO (Figure 8a). The corresponding selected area electron diffraction (SAED) pattern reveals that the hollow spheroids are polycrystalline (Figure 8b). A single point on a representative cocoon (Figure 9a and b), the total area of only one full cocoon (Figure 9c and d), and an area of $25\times17\ \mu m^2$ bearing more than 500 nanococoons (Figure 9e and f) have been se-

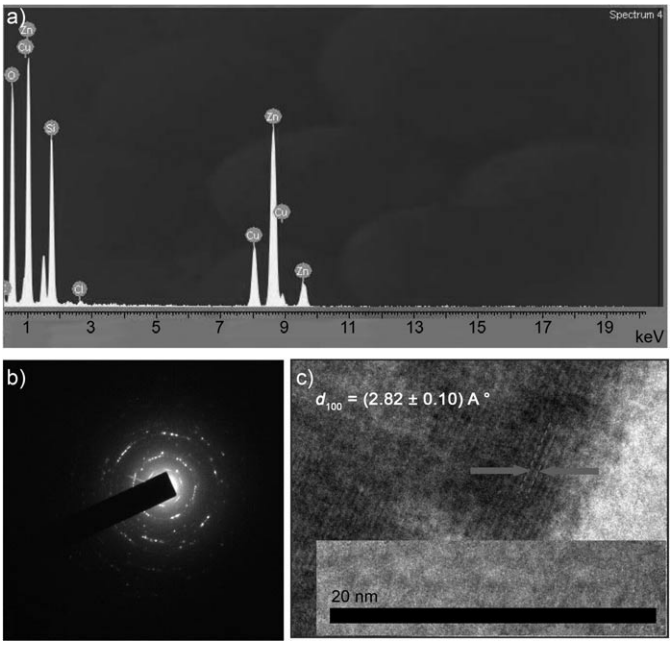

Figure 8. The EDS spectrum of ZnO nanococoon spheroids on a TEM grid (a), the SAED pattern (b), and lattice fringe (c) of a ZnO nanococoon structure.

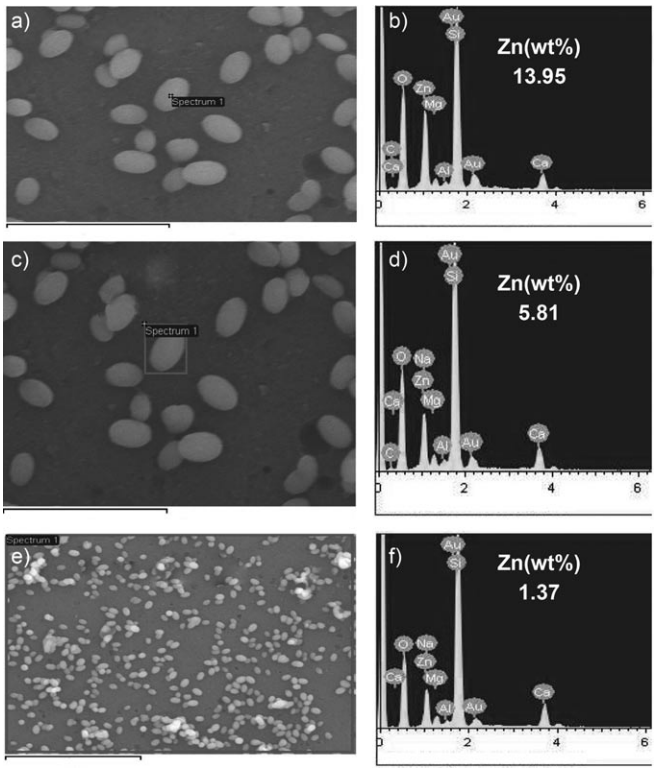

Figure 9. The EDS pattern of ZnO thin film (right) on the glass surface together with the corresponding SEM images (left) for a single scan (a (scale bar = 3 μm), b), a single NC scan (c (scale bar = 3 μm), d), and an area scan (e (scale bar = 10 μm), f).

lectively chosen to gather EDS information to quantify the amount of Zn (in wt %) in the ZnO thin films.

The N_2 adsorption–desorption isotherm and the pore size distribution of ZnO hollow spheroids are shown in Figure 10 and confirm the presence of porous structures of the prepared ZnO hollow spheroids. Here the packing of the ZnO molecules changes because of the thermal effect, which causes a variation in pore size. The BET specific surface area and the average pore size of the ZnO hollow spheroids were around 27.42 $m^2 g^{-1}$and 181.8 nm, respectively, whereas those of the commercial ZnO powders were 3.64 $m^2 g^{-1}$and 28.9 nm, respectively. The experimental findings show a larger specific surface area and average pore size for the ZnO hollow cocoons than the commercial ZnO powder. The SEM and TEM studies authenticate the porous nature of the cocoons and the images also show that the building blocks are not tightly adhered to each other.

Growth mechanism: In the modified hydrothermolysis (MHT) reaction vessel, the synthesis of ZnO nanocrystals involves the hydrolysis of $Zn(CH_3COO)_2$ in a basic pyridine medium. The use of different growth controlling/condensation agents, such as pyridine, triethylamine, and hexamethylenetetramine (HMT), provide the basic conditions required. These agents are small molecules and do not exert the driving force to construct well-organized 1D architectures, especially in the presence of acetate ions. Moreover,

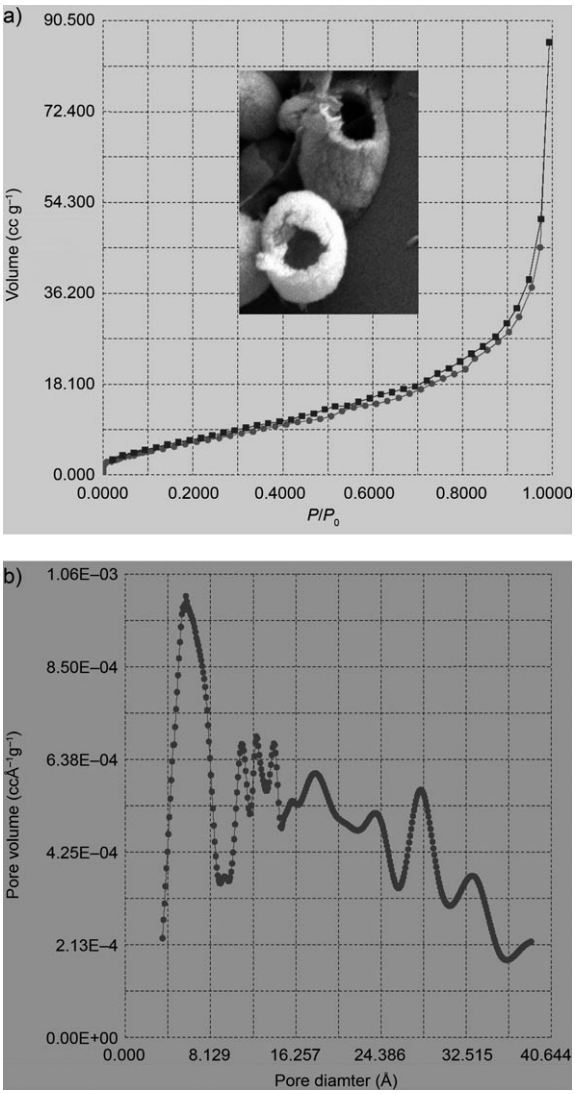

Figure 10. Nitrogen adsorption–desorption isotherm of ZnO nanococoon spheroids (a) and the BJH pore size distribution (b).

very high temperatures (> 100 °C) are avoided to prevent nanorod formation. Thus, a bulb (100 or 200 W) ably supplies sufficient thermal energy for the selective nanococoon structure formation. It may be said that an insignificant fluctuation of temperature has no clear effect under the proposed conditions (both bulbs were found to produce products with the same structural identity). The product ZnO is mainly arranged on the air bubbles (produced by heat treatment) and forms nanococoon architectures. Under the experimental conditions, $Zn(CH_3COO)_2$ molecules become vulnerable to hydrolysis due to the presence of the basic additives, generating the $Zn(OH)_2$ intermediate. Formation of the intermediate may be noted by the characteristic appearance of the turbidity owing to the transient $Zn(OH)_2$ formation in the reaction mixture. The $Zn(OH)_2$ intermediate then suffers dehydration under slow but prolonged ($\approx$12 h) thermal heating to form ZnO hexagons that share edges (from Raman and XRD studies Figure 3). As known, under

heated, basic conditions, dehydration takes place. The ZnO crystal structure has hexagonal close packing of O and Zn atoms in the space group *P*63*mc* with Zn atoms in tetrahedral sites and an inherent asymmetry along the *c* axis. As a result, hexagonal crystals of wurtzite-phase ZnO are formed because of the oriented growth along the (100) plane (Figure 8c). The smaller growth-controlling agents, such as pyridine, triethylamine, and HMT, make the pH high enough for crystal formation. So too many ZnO nuclei as the dehydration product of $Zn(OH)_2$ appear simultaneously at the beginning of the reaction. These nuclei congregate through the dehydration process in a quasi-global manner, and further growth of ZnO nuclei gives ZnO quasi-spheres surrounding the bubbles, as evidenced by the large number of cocoons formed (Figure 5 and Figure S3 in the Supporting Information). Under the prevailing pressure, stationary air or steam bubbles act as soft templates. Heating the reaction mixture in an open pot does not give rise to any cocoon structures.

When the reaction mixture suffers hydrolysis, the bubbles support the orientation of the metallic oxide nanostructures to generate oxide materials without any crystal defects. In $Zn(CH_3COO)_2$, each Zn^{II} ion, because of its inherited octahedral geometry, is coordinated to two CH_3COO^- ions and bridged by two O atoms to form octahedral structures that are connected to each other. These important characteristics help to build a complex architecture based on the hydrolysis of $Zn(CH_3COO)_2$ molecules. In the synthesis presented here, CH_3COO^- ions in $Zn(CH_3COO)_2$ are subsequently replaced by water molecules under basic (pyridine) MHT conditions through a ligand-exchange reaction. There remains enough water bubbles under the prevailing temperature and pressure conditions of MHT in which soft templates, that is, bubbles, act as a catalyst. The self-assembly of hexagonal crystallites driven by the interfacial energy minimization pathway generates blistered aggregates in 2 h (Figure 11a and b) with lower amounts of ZnO. It can be stated that ZnO formation is facile and dehydration starts from the very beginning. The ZnO crystals slowly feed to the periphery of the bubbles accumulating enough ZnO, which finally led to hierarchical hollow cocoons from sufficient amounts of ZnO crystals. The congregation starts after 5 h and is completed in approximately 12 h (Figure 11c–f). Thus distinct nanococoon assembly is observed (Scheme 1). Further heating for longer times (>12 h) caused no deterioration of the cocoons. A similar gas or O_2 bubble has also been exploited as a template for TiO_2 and ZnSe hollow nanostructures.[12] On the other hand, the HMT-promoted hydrolysis reaction allowed the building of the 2D structure in a MHT reaction vessel under a 100 W bulb. Different growth-controlling agents have different basicities and different adsorption capacities on the various facets of ZnO, leading to different growth rates for different crystal facets. Further experiments with HMT also lend support to this proposed mechanism in which ZnO predominantly evolves plates and then cocoons because of the change in basicity of the HMT reaction (Figure S4c and d in the Supporting Information).

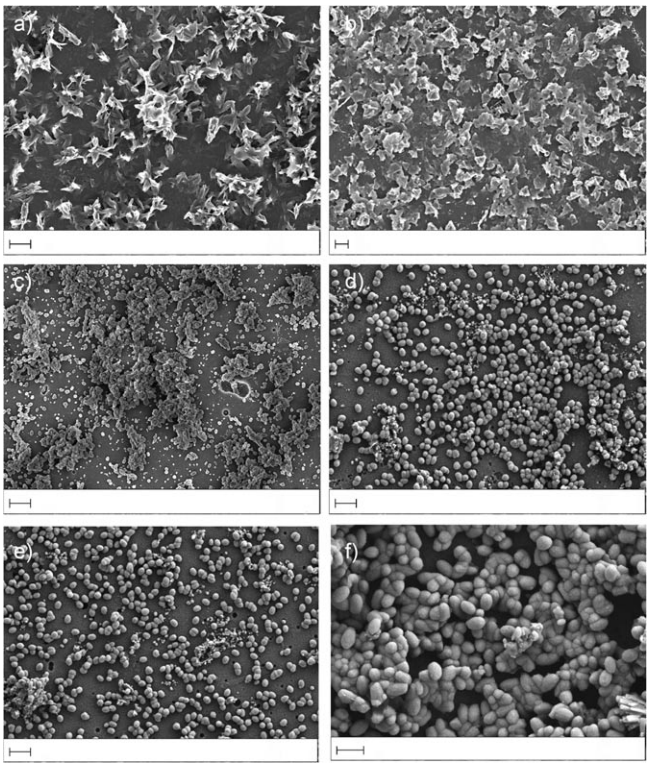

Figure 11. The evolution of a nanococoon structure (time-dependent evolution) through the blister aggregates of ZnO crystals after 1 (a), 2 (b), 5 (c), 8 (d), 10 (e), and 12 h (f). Scale bars: a) 2 μm, b) 2 μm, c) 2 μm, d) 2 μm, e) 2 μm, and f) 1 μm.

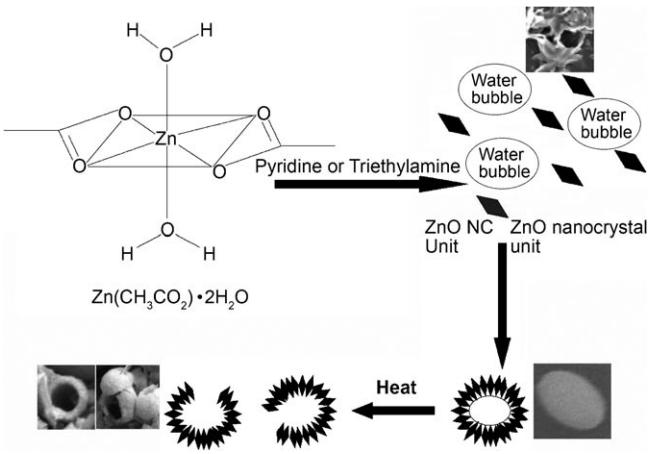

Scheme 1. Probable reaction mechanism for the formation of ZnO nanococoon structures in the MHT reaction vessel.

The present hierarchical structures could not be obtained when using other precursor salts of zinc. Moreover, the reaction temperatures, as well as the amount of weak base, have significant effects. The heterocyclic base pyridine exclusively helps cocoon formation and by lowering the concentration of pyridine a caterpillar like morphology is built up (Figure S4a and b in the Supporting Information). Constant pressure and temperature conditions in the reaction vessel

retain the in situ generated gaseous bubbles, which play an important role in determining the morphology of the spheroids. Ordinary reflux or boiling conditions could not generate such hierarchical nanostructures. Thus a 100 or 200 W tungsten bulb supplies the best heat source in the prescribed MHT reaction vessel. By the reasonable selection of precursors and adjusting other factors, the cocoon morphology of ZnO is controlled.

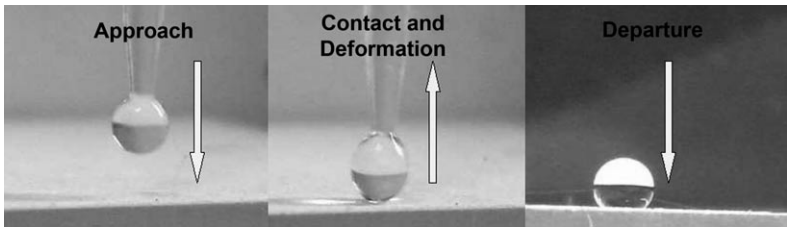

Figure 13. The approach, contact, deformation, and departure processes of a 10 μL water droplet.

Hydrophobicity and hydrophilicity studies: The wettability was evaluated by the water CA measurement for the as-prepared films. Figure 12 shows a spherical water droplet with a

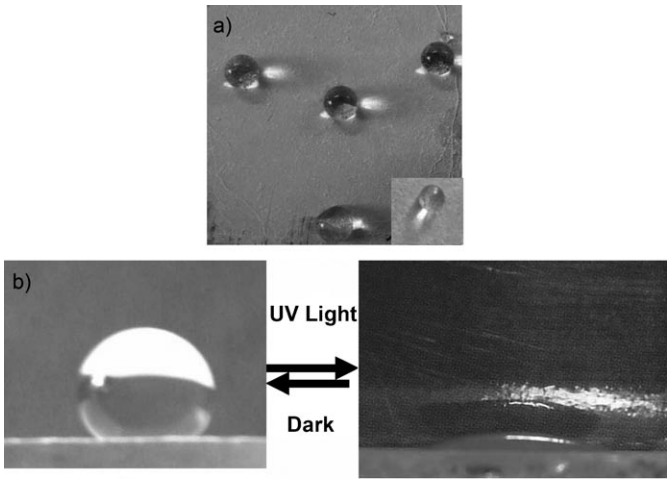

Figure 12. A water droplet on a ZnO thin film (a) and a UV-light switchable superhydrophobic/hydrophilic ZnO surface (b).

water CA of 150°. Upon UV irradiation for 3 h, the water droplet spread out on the film, resulting in a CA of about 0–15° (Figure 12b). This result indicates that the wettability changes from superhydrophobic to superhydrophilic. After UV irradiation the films were kept in the dark for two months and then a new water droplet was used to measure the surface wettability. The superhydrophobicity of the films with nanococoon structures have been reconfirmed in a similar way. This process was repeated several times, and good reversibility of the surface wettability was observed. Figure 13 shows the approach, contact, deformation, and departure processes of a 10 μL water droplet dispensed from a syringe onto the ZnO thin film surface. The high water CA of the as-prepared films, however, indicates that the water droplet does not penetrate or spread, but only remains in contact with the nanococoon structure. Air pockets in the novel 3D nanococoon structure resist water penetration. The large fraction of air trapped in the nanococoon structure forms a cushion at the film–water interface that prevents the penetration of the water droplet into the grooves or cavity of the nanostructure. The presence of grooves or nanocavities in the ZnO nanococoon structures is shown in the FESEM image. When the as-prepared films were irradiated under UV light, their hydrophobic property is transformed and the surface becomes superhydrophilic. This remarkable surface wettability transition can be tuned reversibly.[13] When a water droplet touches the UV illuminated or irradiated film it swells immediately leaving an irregular shape on the surface with a CA of 0–15°. This leads to the conclusion that UV illumination has created a surface that is highly superhydrophilic. Even after storage in the dark for two months, the superhydrophobicity of the ZnO surface reappears.[14] A longer storage period induced a gradual increase in the water CA, revealing a surface wettability trend towards hydrophobicity. This process was repeated for several cycles; a good reversibility of the surface wettability was observed (Figure S5 in the Supporting Information).

ZnO is a photosensitive material and under ultraviolet irradiation may create surface oxygen vacancies at bridging sites, resulting in the conversion of relevant Zn^{II} sites to Zn^{I} sites,[15] which are favorable for dissociative water adsorption. This greatly improves the surface hydrophilicity. For the as-prepared multiscale rough surface, due to presence of the nanococoon structure, the water droplets fill the grooves along the nanococoon structure and replace the trapped air. This results in a water CA of about 0–15°. After the hydroxyl group adsorption, the surface transforms into an energetically metastable state, and the adsorbed hydroxyl groups can gradually be replaced by atmospheric oxygen when the films are placed in the dark.[16] Subsequently, the surface reverts back to its original state, and the surface wettability returns from hydrophilic to -phobic again.

Photocatalytic activity and RhB decolorization: We have investigated the photocatalytic activity of the as-obtained ZnO hollow cocoons in which the light-assisted degradation of RhB, a model water contaminant, has been studied. Under dark conditions and with diffuse light, the RhB content did not change when ZnO samples were employed. Illumination in the absence of ZnO samples did not result in the photocatalytic decolorization of RhB. Therefore, the presence of both UV-light illumination and ZnO samples were necessary for efficient degradation. These results also suggest that the degradation of RhB in aqueous solution is caused by the photocatalytic reactions on ZnO samples

under UV illumination. The characteristic absorption peak of RhB appears at $\lambda = 553$ nm and was chosen to monitor the photocatalytic degradation process. Figure 14a shows

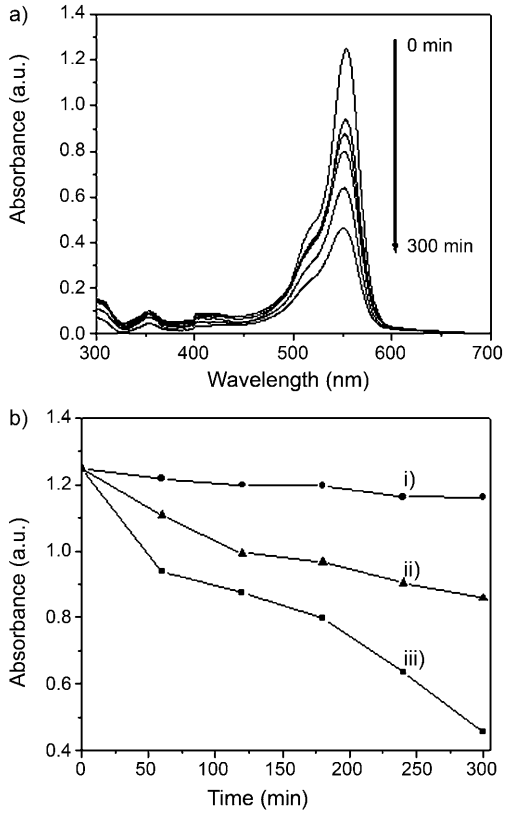

Figure 14. The UV-visible spectra of RhB under UV irradiation (a), and the successive degradation and photodegradation kinetics (b) in the presence of ZnO nanococoon (iii), ZnO solid particle (ii), and without ZnO (i).

the change in the absorption spectrum of an aqueous solution of RhB exposed to UV light for different time periods in the presence of the prepared ZnO sample. The absorption peak at $\lambda = 553$ nm gradually decreases with time upon UV exposure. No new absorption band appears in either the visible or ultraviolet region, which indicates the complete photocatalytic degradation of RhB aqueous solution during the photoreaction. Usually, the complete mineralization of RhB requires a long time (about 48 h) due to the fact that its mineralization goes through two different stages: the ring cleavage in the initial photocatalytic degradation stage and subsequent oxidation of the fragments in the latter stage.[16] This is probably due to the fact that the hollow spheroids possess an unusual hierarchically nanoporous structure, which allows more efficient transport for the reactant molecules to come into contact with the active sites of the nanococoon framework walls, hence enhancing the efficiency of photocatalysis. Moreover, the hollow spheroids allow multiple reflections of UV-visible light within the interior cavity that also facilitates more efficient usage of the light source than solid ZnO particles (Figure 14b). Experiments also show that hollow spheroids can be more readily separated from the slurry system by filtration or decantation after photocatalytic reaction due to their large weight and weak Brownian motion, and the solid catalyst can then be reused. After six repeated cycles of photodegradation of RhB with the as-prepared ZnO, the catalyst retains its original photocatalytic activity, confirming ZnO hollow spheroids are not photocorroded or poisoned during the photocatalytic oxidation of the pollutant dye molecules at a central pH environment (pH $\approx$ 7.0). The most interesting point is that the morphology of the nanostructures remains intact even after the catalysis, as shown in Figure 15. The stability of a photocatalyst is important for its practical application. Therefore, the prepared ZnO hollow spheroids can be regarded as ideal photocatalysts for environmental purification on the industrial scale at a central pH environment. To the best of our knowledge, this is the first report of a one-pot preparation and the photocatalytic activity of hierarchically nanoporous ZnO hollow spheroids. We believe that the prepared ZnO hollow spheroids would be of great interest in solar cell applications, catalysis, separation technology, biomedical engineering, and nanotechnology.

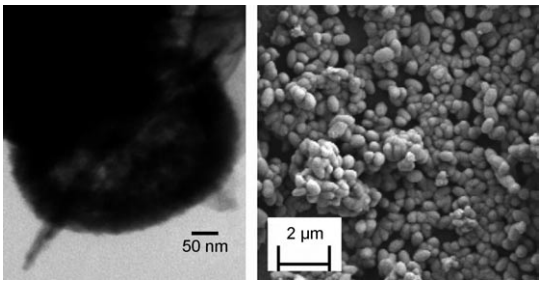

Figure 15. A ZnO nanococoon structure (image TEM and FESEM) after six photocatalytic reaction cycles.

Conclusion

We have synthesized ZnO hierarchical hollow spheroids using $Zn(CH_3COO)_2{\cdot}2H_2O$ as the precursor. A bubble-template strategy is proposed through a MHT reaction to construct hollow ZnO nanostructures. The simple, general, clean, and convenient method presented herein could generate desirable nanostructures with high purity and good crystallinity. Due to the 3D nanococoon architecture, there is improved superhydrophobic and photocatalytic performances. We believe that the present work will open up the way to systematically explore methods to fabricate hollow nanostructures and thus would find usage in a variety of applications.

Experimental Section

General: All the reagents were of AR grade. Triple-distilled water was used throughout the experiments. $Zn(CH_3COO)_2{\cdot}2H_2O$ and RhB were obtained from E-Merck. Pyridine, triethylamine, and hexamethylenetetramine were obtained from Sisco Research Laboratories. All the reagents were used without further purification. Glass slides and beakers were purchased from Blue Star India and were cleaned properly prior to thin-film formation.

All UV/Vis absorption spectra were recorded in a SPECTRASCAN UV 2600 digital spectrophotometer (Chemito, India). XRD was obtained by using a PW1710 diffractometer instrument (Philips, Holland). The XRD data were analyzed by using JCPDS software. Raman spectra were obtained with a Renishaw Raman Microscope, equipped with a He–Ne laser excitation source emitting at a wavelength of $\lambda = 633$ nm, and a Peltier cooled (−70 °C) charge coupled device (CCD) camera. The chemical state of the element on the surface was analyzed by a VG Scientific ESCALAB MK II spectrometer (UK) equipped with an Mg_{KR} excitation source (1253.6 eV) and a five-channeltron detection system. FTIR studies were performed with a Thermo-Nicolet continuum FTIR microscope. Nitrogen adsorption–desorption measurements were performed at 77.3 K by using a quantachrome instrument utilizing the BET model for the calculation of surface areas. The pore size distribution was calculated from the adsorption isotherm curves using the Barrett-Joyner-Halenda (BJH) method. FESEM analysis was performed with a supra 40, Carl Zeiss Pvt. Ltd instrument and an EDS machine (Oxford, Link, ISIS 300) attached to the instrument was used to obtain the nanocrystal morphology and composition . TEM analysis was performed with an instrument H-9000 NAR, Hitachi, using an accelerating voltage of 300 kV.

Synthesis of ZnO nanocrystal thin film on glass: Extremely pure ZnO nanocrystal was synthesized by the modified hydrothermolysis (MHT) of $Zn(CH_3COO)_2{\cdot}2H_2O$ using pyridine or triethylamine as a crystal condensation catalyst. In a typical preparation, aqueous $Zn(CH_3COO)_2$ (2.5 mL, 0.01 M) as precursor solution was mixed with an aqueous solution of pyridine or triethylamine (0.5 mL, 0.1 M) in a screw-capped closed reaction vessel (10.5 cm in length and 1.5 cm in diameter). The mixture was allowed to age for 10–12 h under the illumination of a tungsten bulb (100 W) in a closed wooden box (6×6×7 cm) (Figure 16) to avoid loss of solution during the course of light irradiation. After irradiation, the inner wall of the reaction vessel was uniformly covered with ZnO nanocrystals. In addition to the layer, the reaction vessel accumulates some solid ZnO nanocrystals as a white precipitate. In this way, the deposition of ZnO was done repetitively in the same reaction vessel, as a result of which the thickness of ZnO nanocrystal film was increased through layer-by-layer deposition. In a similar fashion, ZnO nanocrystals were grown on glass slides (1×0.5 cm). The micro slides can be fully covered on both sides by ZnO nanocrystals only when the upper edge of the slide levels off exactly with the air–water interface as the thin film grows favorably from the interface, that is, from the top. The thin-film-covered glass slides or the reaction vessels were washed with water and dried in air and stored in a desiccator.

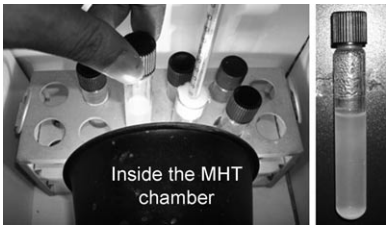

Figure 16. A photograph of the inside of the MHT chamber.

Preparation of ZnO thin-film by drop-casting method: The white solid product from the MHT reaction vessel was washed with pure ethanol and distilled water, then dried under vacuum at room temperature. The ZnO nanocrystals were dispersed in ethanol, and the ethanolic suspension was used to fabricate nanostructured ZnO films by drop casting onto glass slides. Slow evaporation of ethanol led to uniform and total coverage of the glass slides without leaving any vacant space. This thin film has been used throughout the experiment for the hydrophobicity/hydrophilicity experiments.

Measurement of hydrophobicity: Water droplets (10 μL) were carefully dispensed onto the microscopic ZnO nanococoon surfaces prepared on a glass slides by drop-casting techniques and also on the native films obtained after repetitive MHT reaction from the MHT reaction vessel. The average CA value was obtained by measuring at five different positions of the same sample by a digital still camera (Sony Cyber-shot, 8.1 Mega pixels) in a sideways fashion. During this experiment there was no disturbance, such as mechanical jerking or changes in airflow.

Measurement of photocatalytic activity: The evaluation of the photocatalytic activity of the prepared samples for the photocatalytic degradation of an aqueous solution of RhB was performed at ambient temperature (25 °C). The photocatalysis was carried out in a 100 mL beaker. The photo irradiation was done under ordinary germicidal lamps 15 W (Philips, India). The UV lamp emits light predominantly at $\lambda = 365$ nm. Cold water was circulated to avoid heating of the solution in the beaker during the photoreaction. Experiments were as follows: the prepared ZnO powder (0.01 g) was dispersed in an aqueous RhB solution (20 mL, 1×10^{-5} M) in a beaker. The solution was allowed to stand for 30 min to reach an adsorption–desorption equilibrium while admixed with the photocatalyst, before UV irradiation. The average light intensity striking the surface of the reaction solution was about 112 $\mu W\,cm^{-2}$, as measured by a UV meter with the peak intensity of $\lambda = 365$ nm. The concentration of RhB was determined on a UV/Vis spectrophotometer (UV-2550, Chemito, India). After UV irradiation for a prerequisite time span, the concentration change of RhB solution was noted spectrophotometrically. To avoid scattering due to the admixed ZnO nanocrystals in the dye solution, the exposed sample solutions were collected after centrifugation at different time intervals to measure the RhB degradation by using UV/Vis spectroscopy.

Acknowledgements

The authors are thankful to CSIR, UGC, DST, New Delhi and Indian Institute of Technology, Kharagpur, India.

[1] a) H. Zhang, J. Long, A. I. Cooper, *J. Am. Chem. Soc.* **2005**, *127*, 13482; b) H. Gu, R. Zheng, X. Zhang, B. Xu, *Adv. Mater.* **2004**, *16*, 1356; c) S. R. Quake, A. Scherer, *Science* **2000**, *290*, 1536; d) A. Yamaguchi, F. Uejo, T. Yoda, T. Uchida, Y. Tanamura, T. Yamashita, N. Teramae, *Nat. Mater.* **2004**, *3*, 337; e) C. Y. Xu, R. Inai, M. Kotaki, S. Ramakrishna, *Biomaterials* **2004**, *25*, 877; f) X. D. Bai, E. G. Wang, P. X. Gao, Z. L. Wang, *Nano Lett.* **2003**, *3*, 1147; g) J. H. Lim, C. K. Kang, K. K. Kim, I. K. Park, D. K. Hwang, S. J. Park, *Adv. Mater.* **2006**, *18*, 2720; h) P. D. Yang, H. Q. Yan, S. Mao, R. Russo, J. Johnson, R. Saykally, N. Morris, J. Pham, R. R. He, H. J. Choi, *Adv. Funct. Mater.* **2002**, *12*, 323.

[2] a) S. Cheng, D. Yan, J. T. Chen, R. F. Zhuo, J. J. Feng, H. J. Li, H. T. Feng, P. X. Yan, *J. Phys. Chem. C* **2009**, *113*, 13630; b) Z. Gu, M. P. Paranthaman, J. Xu, Z. W. Pan, *ACS Nano* **2009**, *3*, 273; c) Z. Deng, M. Chen, G. Gu, L. Wu, *J. Phys. Chem. B* **2008**, *112*, 16; d) X. Wang, P. Hu, Y. Fangli. , L. Yu, *J. Phys. Chem. C* **2007**, *111*, 6706.

[3] a) R. N. Wenzel, *Ind. Eng. Chem.* **1936**, *28*, 988; b) A. B. D. Cassie, S. Baxter, *Trans. Faraday Soc.* **1944**, *40*, 546; c) R. Blossey, *Nat. Mater.* **2003**, *2*, 301; d) Y. Liu, L. Mu, B. H. Liu, J. L. Kong, *Chem. Eur. J.* **2005**, *11*, 2622; e) I. P. Parkin, R. G. Palgrave, *J. Mater. Chem.* **2005**, *15*, 1689; f) T. L. Sun, L. Feng, X. F. Gao, L. Jiang, *Acc. Chem. Res.* **2005**, *38*, 644.

[4] D. Öner, T. J. McCarthy, *Langmuir* **2000**, *16*, 7777.

[5] L. Feng, S. H. Li, Y. S. Li, H. J. Li, L. J. Zhang, J. Zhai, Y. L. Song, B. Q. Liu, L. Jiang, D. B. Zhu, *Adv. Mater.* **2002**, *14*, 1857.
[6] a) S. Shibuichi, T. Onda, N. Satoh, K. Tsujii, *Langmuir* **1996**, *12*, 2125; b) X. Zhang, F. Shi, X. Yu, H. Liu, Y. Fu, Z. Q. Wang, L. Jiang, X. Y. Li, *J. Am. Chem. Soc.* **2004**, *126*, 3064; c) N. J. Shirtcliffe, G. McHale, M. I. Newton, G. Chabrol, C. C. Perry, *Adv. Mater.* **2004**, *16*, 1929; d) K. K. S. Lau, J. Bico, K. B. K. Teo, M. Chhowalla, G. A. J. Amaratung, W. I. Milne, G. H. McKinley, K. K. Gleason, *Nano Lett.* **2003**, *3*, 1701.
[7] R. Wang, K. Hashimoto, A. Fujishima, M. Chikuni, E. Kojima, A. Kitamura, M. Shimohigoshi, T. Watanabe, *Nature* **1997**, *388*, 431.
[8] M. Moriya, K. Yoshikawa, W. Sakamoto, T. Yogo, *Inorg. Chem.* **2009**, *48*, 8544.
[9] Y. F. Zhu, D. H. Fan, W. Z. Shen, *J. Phys. Chem. C* **2007**, *111*, 18629.
[10] Z. Zhang, M. Lu, H. Xu, W. S. Chin, *Chem. Eur. J.* **2007**, *13*, 632.
[11] S. Major, S. kumar, M. Bhatnagar, K. L. Chopra, *Appl. Phys. Lett.* **1986**, *49*, 394.
[12] a) J. Zhang, L. D. Sun, C. S. Liao, C. H. Yan, *Chem. Commun.* **2002**, 262; b) Q. Peng, Y. Dong, Y. D. Li, *Angew Chem.* **2003**, *115*, 3135; *Angew Chem. Int. Ed.* **2003**, *42*, 3027; c) X. Li, Y. Xiong, Z. Li, Y. Xie, *Inorg. Chem.* **2006**, *45*, 3493.
[13] X. Feng, L. Feng, M. Jin, J. Zhai, L. Jiang, D. Zhu, *J. Am. Chem. Soc.* **2004**, *126*, 62.
[14] H. Liu, L. Feng, J. Zhai, L. Jiang, D. Zhu, *Langmuir* **2004**, *20*, 5659.
[15] L. Huang, S. P. Lau, H. Y. Yang, E. S. P. Leong, S. F. Yu, *J. Phys. Chem. B* **2005**, *109*, 7746.
[16] J. I. Guoyu, X. Yu, *Environ. Sci. Technol.* **2008**, *42*, 4902.
[17] A. K. Sinha, S. Jana, S. Pande, S. Sarkar, M. Pradhan, M. Basu, S. Saha, A. Pal, T. Pal, *CrystEngComm* **2009**, *11*, 1210.

Received: December 6, 2009
Published online: May 21, 2010

